Exceptional-point-engineered cavity magnomechanics

Tian-Xiang Lu, Huilai Zhang, Qian Zhang, and Hui Jing*

Key Laboratory of Low-Dimensional Quantum Structures and Quantum Control of Ministry of Education, Department of Physics and Synergetic Innovation Center for Quantum Effects and Applications, Hunan Normal University, Changsha 410081, China

(Received 18 March 2021; accepted 1 June 2021; published 15 June 2021)

We theoretically study the role of the exceptional point (EP) in a non-Hermitian cavity magnomechanical (CMM) system, with a tunable dissipative magnon-photon coupling. We find that the EP emerging in such a system can radically change the properties of photons and phonons. As a result, flexible on-off optical transmission, coherent switching of slow and fast lights, and enhanced mechanical cooling deep into the ground state can be achievable by approaching the EP. Detailed comparisons between this system and its Hermitian counterpart are given. Our results show that EP-assisted CMM devices can serve as tools for applications in optical communications and electromechanical switching or sensing.

DOI: 10.1103/PhysRevA.103.063708

I. INTRODUCTION

Hybrid quantum systems, such as electronic and optical elements linked through the bridge of mechanical oscillations, play a key role in building quantum networks, especially coherent signal switching or transducing [1]. Another recent example is hybrid magnonic devices involving collective spin excitations of a yttrium-iron-garnet (YIG) sphere [2–17]. In such devices, coherent magnon-photon coupling can be utilized to control spin current [18,19], to achieve quantum entanglement of magnons [20,21], and to observe non-Hermitian effects [22–25]. Furthermore, by coherently coupling photons and magnons and various acoustic motions [26–35], more intriguing applications can be envisaged, i.e., tripartite photon-magnon-phonon entanglement [30–32], ultraslow light engineering [33,34], and magnomechanical sensing [35].

In parallel, exotic properties of dissipative coupling have attracted intense interest in recent years [36–43], which has been observed in cold atoms [36,37], electrical circuits [38], thermal materials [39], and optical devices [40–42]. In particular, based on dissipative coupling of magnons and photons, level attractions of hybridized modes were also demonstrated [44–53]. This opens up a route to make and utilize unconventional magnonic devices such as nonreciprocal light switches [54–56] and non-Hermitian magnonic sensors [57,58]. Inspired by these pioneering works, here we consider a non-Hermitian cavity magnomechanical (CMM) system, with both coherent magnon-phonon coupling and dissipative photon-magnon coupling. In such a system, both eigenvalues and their corresponding eigenvectors are coalesced at the exceptional points (EPs) [59–61], providing a possibility to engineer CMM devices. We note that counterintuitive EP effects have already been demonstrated in diverse systems, such as single-mode lasing [62,63], topological energy transfer [64], wireless electronic power transfer [65], coherent perfect absorption [66–68], and enhanced performance of sensors [69–72]. In this paper, unconventional EP effects are revealed in cavity magnomechanics, including significantly modified optical transmissions, slow-to-fast light transition, and also enhanced mechanical cooling. Our paper confirms that non-Hermitian CMM devices can serve as powerful tools for manipulating photons and phonons, with potential applications in microwave-to-optical conversion [73] or weak magnetic-field sensing [74–77].

II. MAGNOMECHANICALLY INDUCED TRANSPARENCY AT EXCEPTIONAL POINTS

As shown in Fig. 1, we consider a Fabry-Pérot cavity of resonance frequency ω_a and damping rate κ_a, coupled with a YIG sphere. Dissipative magnon-photon coupling in such a system was already realized in recent experiments [45–47]. The YIG sphere glued to the end of a silica fiber is placed near the inner edge at the middle plane of the waveguide. The cavity is aligned in the x direction, while an external magnetic field H is applied in the z direction. Due to the magnetic field, a uniform magnon mode with damping rate κ_m appears in the sphere at the resonance frequency $\omega_m = \gamma H$, where γ is the gyromagnetic ratio. The angular position θ of the YIG sphere can be finely tuned [45–47], leading to dissipative or coherent magnon-photon coupling for $\theta \in (65^\circ, 115^\circ) \cup (-65^\circ, -115^\circ)$ or $\theta \in (-65^\circ, 65^\circ) \cup (115^\circ, 180^\circ] \cup (-115^\circ, -180^\circ]$ [45,46].

The magnetization dynamics of the YIG sphere can be described by the Landau-Lifshitz-Gilbert equation [8,45],

$$\frac{d\mathbf{M}}{dt} = \gamma \mathbf{M} \times \mathbf{H}_t - \frac{\alpha}{M_0} \mathbf{M} \times \frac{d\mathbf{M}}{dt}, \tag{1}$$

where $\mathbf{H}_t = h_x(t)\hat{x} + h_y(t)\hat{y} + H\hat{z}$, $\mathbf{M} = M_x(t)\hat{x} + M_y(t)\hat{y} + M_0\hat{z}$, and $h_{x,y}(t)$ or $M_{x,y}(t)$ is the rf magnetic field or the magnetization, respectively (M_0 is the saturation magnetization). Here this damping term α is assumed to be scalar for uniaxial symmetry and small oscillations (see, e.g., Refs. [78–80]), the value of which can be experimentally obtained [80]. We note that in practice the magnetization damping can be

*Corresponding author: jinghui73@foxmail.com

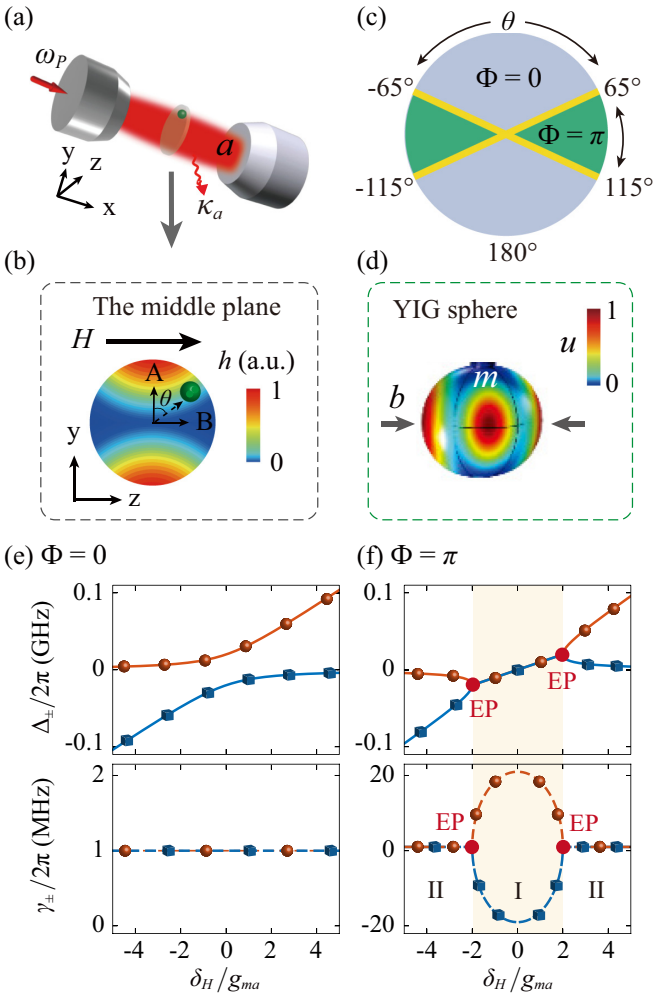

FIG. 1. (a) A non-Hermitian CMM system, with a highly polished YIG sphere inside a microwave cavity, supporting a magnon mode m and a phonon mode b [26,45]. (b) The simulated h field amplitude for the TE_{11} mode at the middle plane of the empty cavity. A or B denotes the h antinode or node position and θ is the angular position of the sphere. (c) The relation between θ and the coupling phase Φ [45]. The measured value of Φ is uncertain for the yellow region, e.g., $\theta \simeq \pm 65^\circ$ or $\pm 115^\circ$ [45]. (d) Simulated mechanical displacement (u) as in the experiment [26]. (e), (f) The hybridized mode eigenfrequencies, $\Delta_\pm = \mathrm{Re}(\omega_\pm) - \omega_a$, as a function of the detuning $\delta_H = \omega_m - \omega_a$ for $\Phi = 0$ or π, respectively. Dashed lines in (e) and (f) denote the linewidths $\gamma_\pm = \mathrm{Im}(\omega_\pm)$.

affected by many factors such as spin pumping, eddy currents, or incoherent scattering of magnons, and for general anisotropic systems a tensor form of damping has been developed in recent works to describe the magnetization relaxation near equilibrium [81–84]. For stronger thermal or mechanical motions, novel anisotropic effects may also be revealed in non-Hermitian CMM systems, e.g., direction-dependent magnomechanically induced transparency (MMIT) or slow light; these new possibilities will be explored in our future works. From this equation, one can derive a simple relation for the microwave current j and magnetization m [45], i.e., $(\omega - \omega_m + i\kappa_m)M - i\omega_r(K_A - K_L)j = 0$, where $\omega_r = \gamma M_0$, and in view of the Ampère law (K_A) and the Lenz law (K_L), $h = h_x + ih_y = h^A + h^L = -i(K_A - K_L)j$. The competition between the terms K_L and K_A leads to a net coherent or dissipative coupling [45]. This equation, along with the RLC circuit (consisting of a resistor, an inductor, and a capacitor) equation [45], $(\omega^2 - \omega_a^2 + i\kappa_a)j + iK_F\omega^2 M = i\omega V_0/L$, with the applied or induced voltage V_0 or $V_F = \mp K_F L dM/dt$, can be written in the form of linearly coupled harmonic oscillators [85]:

$$\begin{pmatrix} \omega^2 - \omega_a^2 + i\kappa_a & i\omega^2 K_F \\ -i\omega_r(K_A - K_L) & \omega - \omega_m + i\kappa_m \end{pmatrix} \begin{pmatrix} j \\ M \end{pmatrix} = 0. \quad (2)$$

Following the standard quantization procedures [45,46,85], denoting the creation (annihilation) operator for the photons and magnons as a ($a^\dagger$) and m ($m^\dagger$), respectively, we can write the non-Hermitian coupling term $\hbar g_{ma}(a^\dagger m + e^{i\Phi} a m^\dagger)$, with [45–47]

$$g_{ma} = \sqrt{\frac{\omega_a \omega_r |K_F(K_A - K_L)|}{2}}, \quad (3)$$

and

$$\Phi = \arctan\left\{\frac{\mathrm{Im}\,[K_F(K_A - K_L)]}{\mathrm{Re}\,[K_F(K_A - K_L)]}\right\}. \quad (4)$$

Since $K_{F,A,L}$ is real positive, we have $\Phi = n\pi$ ($n \in Z$); thus, for $K_A > K_L$ or $K_A < K_L$, we have $\Phi = 0$ (coherent coupling) or $\Phi = \pi$ (dissipative coupling) [45–47]. The relation of the angular position θ to the coupling phase Φ, as shown in Fig. 1(c), was observed in the experiments [45–47]. The eigenfrequencies and eigenvectors of this system are

$$\omega_\pm = \frac{1}{2}\left[\tilde{\omega}_a + \tilde{\omega}_m \pm \sqrt{(\tilde{\omega}_a - \tilde{\omega}_m)^2 + 4g_{ma}^2 e^{i\Phi}}\right], \quad (5)$$

and

$$\begin{pmatrix} \psi_a \\ \psi_m \end{pmatrix} = \begin{pmatrix} g_{ma} \\ (\tilde{\omega}_a - \tilde{\omega}_m)/2 \pm \sqrt{(\tilde{\omega}_a - \tilde{\omega}_m)^2/4 + e^{i\Phi} g_{ma}^2} \end{pmatrix}, \quad (6)$$

where $\tilde{\omega}_{a,m} = \omega_{a,m} - i\kappa_{a,m}$. Figures 1(e) and 1(f) show their dependences on the field detunings $\delta_H = \omega_m - \omega_a$, with experimentally accessible values [44,51] $\omega_a/2\pi = 13.205$ GHz, $g_{ma}/2\pi = 20$ MHz, $\kappa_a/2\pi = 1$ MHz, and $\kappa_m/2\pi = 1$ MHz. We see that the energy levels of the coupled modes repel each other for $\Phi = 0$, while for $\Phi = \pi$ both the eigenfrequencies and the eigenvectors simultaneously coalesce, under the condition $|\delta_H| = 2g_{ma}$ [44,51], featuring the emergence of EPs. In particular, (I) for $|\delta_H| > 2g_{ma}$, we have all real eigenfrequencies, while (II) for $|\delta_H| < 2g_{ma}$, we have complex ones.

We note that the YIG sphere can also support a mechanical breathing mode with the frequency ω_b and the damping rate γ_b [26], based on which MMIT, in analogy to optomechanically induced transparency [86–88], was observed very recently [26]. In a frame rotating at the pump frequency ω_0, with a weak probe field of the frequency ω_p and the amplitudes E_p, the Hamiltonian of such a CMM system can be written in the simplest level as ($\hbar = 1$)

$$\begin{aligned} \mathcal{H} &= \mathcal{H}_0 + \mathcal{H}_{\mathrm{int}} + \mathcal{H}_{\mathrm{dr}}, \\ \mathcal{H}_0 &= \Delta_a a^\dagger a + \Delta_m m^\dagger m + \omega_b b^\dagger b, \\ \mathcal{H}_{\mathrm{int}} &= g_{ma}(a^\dagger m + e^{i\Phi} a m^\dagger) + g_{mb} m^\dagger m(b + b^\dagger), \\ \mathcal{H}_{\mathrm{dr}} &= i(E_{dr} m^\dagger + E_p e^{-i\xi t} a^\dagger - \mathrm{H.c.}), \end{aligned} \quad (7)$$

where $\Delta_a = \omega_a - \omega_0$, $\Delta_m = \omega_m - \omega_0$, and $\xi = \omega_p - \omega_0$. b or $b^\dagger$ is the annihilation or creation operator of the phonon mode, respectively, and g_{mb} is the coupling rate with typical values $4 \leqslant g_{mb}/2\pi \leqslant 60\,\text{mHz}$ [26]. In particular, for $g_{mb} = 0$, the whole system can be reduced to a cavity magnonic (CM) system [45–47]. For $g_{mb} \neq 0$ and $\Phi = 0$, the whole system can be reduced to a Hermitian CMM system [26]. For experimentally accessible parameter values, the ratio of magnon-phonon coupling to magnon-photon coupling, i.e., g_{mb}/g_{ma}, is $\approx 10^{-9}$. Thus, in such a system, only the lowest EP exists, without the need to consider any higher-order EPs [89]. $E_{dr} = \frac{\sqrt{5}}{4}\gamma\sqrt{N}B_0$ is the drive strength with the field amplitude B_0, the frequency ω_0, and the total number of spins $N = \rho V$, with $\rho = 4.22 \times 10^{27} m^{-3}$ (ρ is the spin density and V is the volume of the sphere) [29–32].

The Heisenberg equations of motion (EOM) of the system are then

$$\begin{aligned}
\dot{m} &= -(i\Delta_s + \kappa_m)m - ig_{ma}ae^{i\Phi} + E_{dr}, \\
\dot{a} &= -(i\Delta_a + \kappa_a)a - ig_{ma}m + E_p e^{-i\xi t}, \\
\dot{b} &= -(i\omega_b + \gamma_b)b - ig_{mb}m^\dagger m,
\end{aligned} \tag{8}$$

where

$$\Delta_s = \Delta_m + g_{mb}(b_s + b_s^*).$$

Typically, the MMIT process can be well treated in the semiclassical (instead of quantum) perturbation framework [90]. For a probe field much weaker than the pump, we expand every operator as the sum of its steady value and a small fluctuation, i.e., $o(t) = o_s + \delta o$, where $o(t)$ denotes any one of these quantities $a(t)$, $b(t)$, and $m(t)$. Then we have the steady-state values of the dynamical variables:

$$\begin{aligned}
m_s &= \frac{-ig_{ma}a_s e^{i\Phi} + E_{dr}}{i\Delta_s + \kappa_m}, \\
a_s &= \frac{-ig_{ma}m_s}{i\Delta_a + \kappa_a}, \quad b_s = \frac{-ig_{mb}|m_s|^2}{i\omega_b + \gamma_b}.
\end{aligned} \tag{9}$$

Also, it is straightforward to show that $|m_s|^2$ satisfies

$$|m_s|^2\left(\Delta_s^2 + \kappa_m^2\right) = \left|-ig_{ma}e^{i\Phi}a_s + E_{dr}\right|^2, \tag{10}$$

which can be recast as

$$a_3 x^3 + a_2 x^2 + a_1 x + a_0 = 0, \tag{11}$$

with $x = |m_s|^2$ and the coefficients

$$\begin{aligned}
a_3 &= 4g_{mb}^2\omega_b^2\eta_a, \quad a_2 = 4g_{mb}^2\alpha\omega_b\left(g_{ma}^2\mu_a - \Delta_m\eta_a\right), \\
a_1 &= 2g_{ma}^2\alpha^2(\kappa_a\beta - \Delta_a\mu_m) + \eta_a\eta_m\alpha^2 + g_{ma}^4\alpha^2, \\
a_0 &= -\eta_a\alpha^2 E_{dr}^2,
\end{aligned} \tag{12}$$

and

$$\begin{aligned}
\alpha &= \omega_b^2 + \gamma_b^2, \quad \eta_{a,m} = \Delta_{a,m}^2 + \kappa_{a,m}^2, \\
\beta &= \kappa_m\cos(\Phi) + \Delta_m\sin(\Phi), \\
\mu_{a,m} &= \Delta_{a,m}\cos(\Phi) - \kappa_{a,m}\sin(\Phi).
\end{aligned}$$

Figures 2(a) and 2(b) show the mean magnon number $|m_s|^2$ versus the microwave drive field amplitude B_0 for different δ_H. Taking the case $\delta_H/g_{ma} = -4$ and $\Phi = \pi$ for an example, when $0.57 < B_0 < 2.66\,\text{mT}$, Eq. (11) has three solutions, which means the system enters the bistable regime. In order to study MMIT, this system should be in the stable regime ($B_0 < 0.57\,\text{mT}$) where Eq. (11) only has a single real solution. Thus for $-4 \leqslant \delta_H/g_{ma} \leqslant 4$ and $\Phi = \{0, \pi\}$ in this paper, B_0 is set to 0.5 mT.

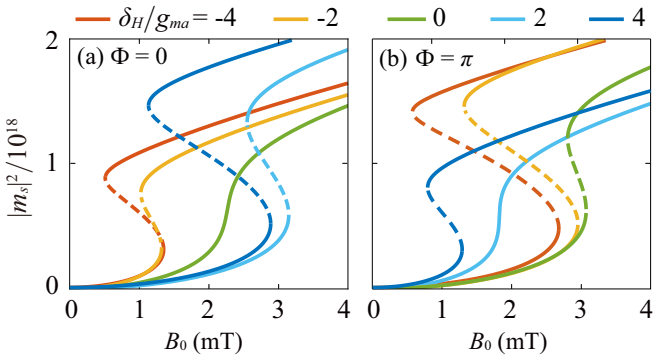

FIG. 2. Numerical solutions of Eq. (11). Mean magnon number $|m_s|^2$ is plotted as a function of the drive field amplitude B_0 for different δ_H/g_{ma}. Φ is set to zero (a) and π (b), respectively. The other parameters can be found in the main text.

Now we consider the perturbation induced by the input probe field. After eliminating the steady-state values and neglecting the higher-order terms, we obtain the linearized EOM:

$$\begin{aligned}
\delta\dot{a} &= -(i\Delta_a + \kappa_a)\delta a - ig_{ma}\delta m + E_p e^{-i\xi t}, \\
\delta\dot{m} &= -(i\Delta_s + \kappa_m)\delta m - ig_{mb}m_s(\delta b + \delta b^\dagger) - ig_{ma}e^{i\Phi}\delta a, \\
\delta\dot{b} &= (i\omega_b + \gamma_b)\delta b - i(g_{mb}m_s^*\delta m + g_{mb}m_s\delta m^\dagger).
\end{aligned} \tag{13}$$

Using the ansatz

$$\begin{pmatrix}\delta a \\ \delta m \\ \delta b\end{pmatrix} = \begin{pmatrix}\mathcal{A}_- \\ \mathcal{M}_- \\ \mathcal{B}_-\end{pmatrix}e^{-i\xi t} + \begin{pmatrix}\mathcal{A}_+ \\ \mathcal{M}_+ \\ \mathcal{B}_+\end{pmatrix}e^{i\xi t}, \tag{14}$$

the solution for $\mathcal{A}_-$ corresponding to the input probe field $E_p e^{-i\xi t}$ is

$$\mathcal{A}_- = \frac{[\mathcal{K}_3(\xi) + \mathcal{G}_-\mathcal{K}_4(\xi)]E_p}{\mathcal{F}_1(\xi)\mathcal{K}_3(\xi) + \mathcal{F}_5(\xi)\mathcal{F}_6(\xi)\mathcal{K}_2(\xi) + \mathcal{K}_1(\xi)}, \tag{15}$$

with $\mathcal{G}_\pm = g_{ma}^2 e^{\pm i\Phi}$, and

$$\begin{aligned}
\mathcal{F}_{1,2}(\xi) &= -i\xi \pm i\Delta_a + \kappa_a, \\
\mathcal{F}_{3,4}(\xi) &= -i\xi \pm i\Delta_s + \kappa_m, \\
\mathcal{F}_{5,6}(\xi) &= -i\xi \pm i\omega_b + \gamma_b, \\
\mathcal{K}_1(\xi) &= 2i\omega_b|G|^2[\mathcal{F}_2(\xi)\mathcal{G}_+ - \mathcal{F}_1(\xi)\mathcal{G}_-], \\
\mathcal{K}_2(\xi) &= \mathcal{F}_1(\xi)\mathcal{F}_3(\xi)\mathcal{G}_- + \mathcal{F}_2(\xi)\mathcal{F}_4(\xi)\mathcal{G}_+ + g_{ma}^4, \\
\mathcal{K}_3(\xi) &= \mathcal{F}_2(\xi)\mathcal{F}_3(\xi)\mathcal{F}_4(\xi)\mathcal{F}_5(\xi)\mathcal{F}_6(\xi) - 4\mathcal{F}_2(\xi)\omega_b\Delta_s|G|^2, \\
\mathcal{K}_4(\xi) &= \mathcal{F}_3(\xi)\mathcal{F}_5(\xi)\mathcal{F}_6(\xi) - 2i\omega_b|G|^2.
\end{aligned}$$

Here $G = g_{mb}m_s$ is the effective magnomechanical coupling coefficient. Then with the aid of the input-output relation [91]

$$a_{\text{out}} = a_{\text{in}} - \sqrt{2\kappa_{\text{ex}}}\mathcal{A}_-, \tag{16}$$

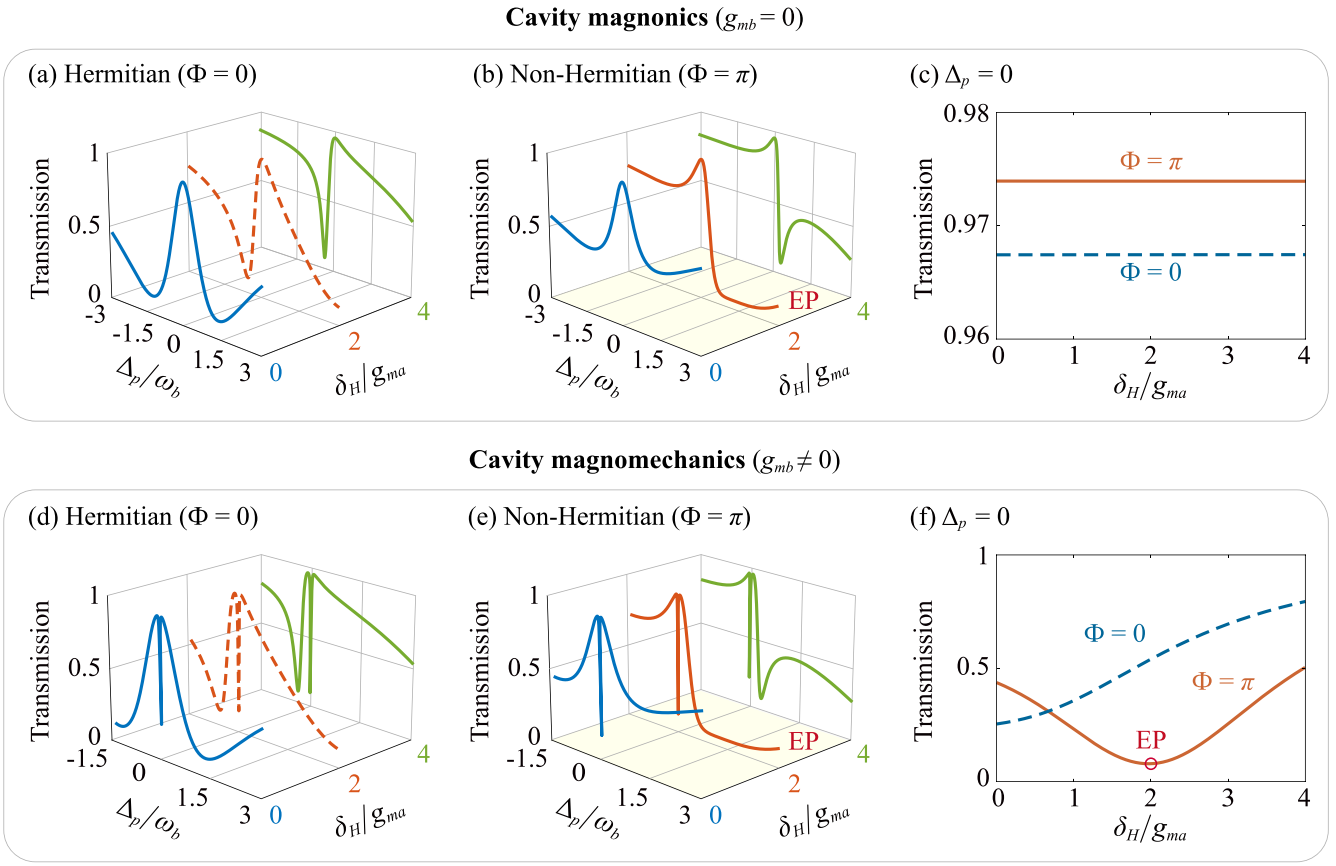

FIG. 3. Transmission rate of the probe light as a function of the field detuning δ_H and the probe detuning $\Delta_p = \xi - \omega_b$ for $g_{mb} = 0$ ((a)–(c), corresponding to a CM system [45–47]) and $g_{mb} \neq 0$ ((d)–(f), corresponding to a CMM system [26]). (e) For $g_{mb} \neq 0$ and $\Phi = \pi$, transmission rate of the probe light as a function of δ_H and Δ_p, corresponding to a non-Hermitian CMM system. (f) Transmission rate of the probe light as a function of δ_H with different values Φ. In these figures, we have selected $B_0 = 0.5$ mT. See the text for the other parameter values.

where $\kappa_{\rm ex}$ is the external loss rate and $a_{\rm in}$ ($a_{\rm out}$) is the input (output) probe amplitudes, we can obtain the transmission rate of the probe field as

$$T = |t_p|^2 = \left|\frac{a_{\rm out}}{a_{\rm in}}\right|^2 = \left|1 - \frac{2\kappa_{\rm ex}\mathcal{A}_-}{E_p}\right|^2. \tag{17}$$

With this at hand, we can discuss the EP effects on the MMIT process and accompanying group delay. In numerical simulations, we have selected experimentally feasible parameters [26,45], i.e., $\omega_a/2\pi = 13.205$ GHz, $g_{ma}/2\pi = 20$ MHz, $\kappa_a/2\pi = 1$ MHz, $\kappa_m/2\pi = 1$ MHz, $\omega_b/2\pi = 15$ MHz, $\gamma_b/2\pi = 300$ Hz, and $g_{mb}/2\pi = 9.9$ mHz.

Figure 3 shows the transmission rate of the probe light as a function of δ_H and Δ_p. As shown in Figs. 3(a) and 3(b), when $g_{mb} = 0$ (CM system), a magnetically induced transparency (MIT) window appears, and a Fano-like shape can be observed in the spectra by varying field detuning δ_H [6,25,45,47] for both $\Phi = 0$ and π. At the resonance point $\Delta_p = 0$, the variation of δ_H leads to subtle changes in the spectra [see Fig. 3(c)]. As for $g_{mb} \neq 0$ (the CMM system), in contrast to MIT, double transparency windows appear in the transmission spectra due to the presence of the phonon mode [26], as shown in Figs. 3(d) and 3(e). What is more, for $g_{mb} \neq 0$ and $\Phi = \pi$ (the non-Hermitian CMM system), the transmission rate at $\Delta_p = 0$ first drops down and then increases with further increasing δ_H, with a turning point corresponding to the EP [see Fig. 3(f)]. This turning behavior cannot be observed in the CMM system without the EP [see the blue curve in Fig. 3(f)], which implies that, by tuning δ_H to surpass EPs, the transmission of the probe light can be absorbed or reflected by the system, opening up an avenue to utilizing EP-assisted CMM devices in coherent optical communications [92–94].

Accompanying the MMIT process, dramatic reduction in the optical group delay can emerge in such a system [95,96], due to the rapid variation of the refractive index in the MMIT process, which is characterized by

$$\tau_g = \frac{d\arg(t_p)}{d\Delta_p}. \tag{18}$$

Figure 4 shows that τ_g can be tuned by changing the phase factor Φ (i.e., the YIG sphere location) or the field detuning δ_H. For $\delta_H = 0$, the group delay can be tuned to be positive or negative, i.e., controllable switching from fast to slow light is achievable by tuning Φ. Moreover, by changing the field detuning δ_H, the system can also switch from slow to fast light in the vicinity of the EPs [92–94]. The fact that the presence of EPs can strongly modify the dispersion of the system provides

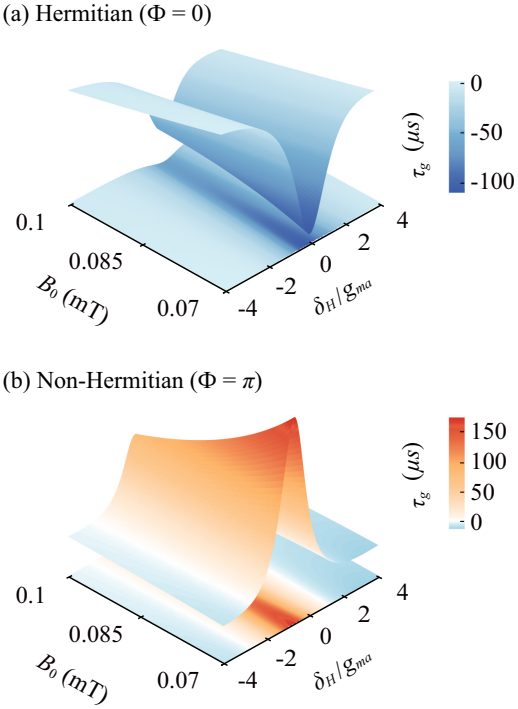

FIG. 4. Group delay of the probe light τ_g as a function of the field detuning Δ_H and the drive field amplitude B_0 for $\Phi = 0$ (a) and $\Phi = \pi$ (b). In these figures, we have selected $\Delta_p = 0$. See the text for the other parameter values.

a powerful way to slow or advance signals by using such a non-Hermitian CMM device.

III. MECHANICAL COOLING AT EPs

Now we theoretically study the role of EPs in further enhancing mechanical cooling in the non-Hermitian CMM system. We find that in comparison with the Hermitian CMM system a factor 2 enhancement of the cooling rate is achievable near the EP, resulting in a lower phonon number, i.e., $n_f \simeq 0.22$. To see this, we consider the effective linearized Hamiltonian of the fluctuation operators (hereafter we drop the notation δ for all the fluctuation operators for the sake of simplicity, like $\delta a \to a$):

$$H_{\rm eff} = \Delta_a a^\dagger a + \Delta_s m^\dagger m + g_{ma}(a^\dagger m + e^{i\Phi} a m^\dagger) + \omega_b b^\dagger b + G(m + m^\dagger)(b + b^\dagger), \tag{19}$$

where $\Delta_s = \Delta_m + g_{mb}(b_s + b_s^*)$ and $G = g_{mb} m_s$. In the weak-coupling regime, the reaction of the mechanical resonator to the magnon can be neglected. So the fluctuation spectrum $S_{FF}(\omega)$ of the magnetostrictive force $F = m + m^\dagger$ is totally determined by the optical and magnetic part in the effective Hamiltonian Eq. (19),

$$H_{\rm ma} = \Delta_a a^\dagger a + \Delta_s m^\dagger m + g_{ma}(a^\dagger m + e^{i\Phi} a m^\dagger), \tag{20}$$

and the linearized quantum Langevin equations are given by

$$\begin{aligned} \dot a &= -(i\Delta_a + \kappa_a)a - i g_{ma} m + \sqrt{\kappa_a}\, a_{\rm in}, \\ \dot m &= -(i\Delta_s + \kappa_m)m - i g_{ma} e^{i\Phi} a + \sqrt{\kappa_m}\, m_{\rm in}, \end{aligned} \tag{21}$$

where $a_{\rm in}$ and $m_{\rm in}$ are the noise operators satisfying

$$\begin{aligned} \langle a_{\rm in}(t) a_{\rm in}^\dagger(t')\rangle &= \delta(t - t'), \\ \langle m_{\rm in}(t) m_{\rm in}^\dagger(t')\rangle &= \delta(t - t'). \end{aligned} \tag{22}$$

In the frequency domain, the linearized quantum Langevin equations are written as

$$\begin{aligned} -i\omega a(\omega) &= -(i\Delta_a + \kappa_a)a(\omega) - i g_{ma} m(\omega) \\ &\quad + \sqrt{\kappa_a}\, a_{\rm in}(\omega), \\ -i\omega m(\omega) &= -(i\Delta_s + \kappa_m)m(\omega) - i g_{ma} e^{i\Phi} a(\omega) \\ &\quad + \sqrt{\kappa_m}\, m_{\rm in}(\omega). \end{aligned} \tag{23}$$

As a result, we obtain

$$S_{FF}(\omega) = \frac{1}{A(\omega)} + \frac{1}{A^*(\omega)}, \tag{24}$$

with

$$A(\omega) = \kappa_m - i(\omega - \Delta_s) + \frac{g_{ma}^2 e^{i\Phi}}{\kappa_a - i(\omega - \Delta_a)}.$$

Following the methods as given in Refs. [97,98], we can obtain the rate equations of the mechanical mode as

$$\begin{aligned} \dot P_n &= \Gamma_{n\leftarrow n+1} P_{n+1} + \Gamma_{n\leftarrow n-1} P_{n-1} - \Gamma_{n-1\leftarrow n} P_n - \Gamma_{n+1\leftarrow n} P_n \\ &\quad + \gamma_b(n_m + 1)(n + 1)P_{n+1} + \gamma_b n_m n P_{n-1} \\ &\quad - \gamma_b(n_m + 1)n P_n - \gamma_b n_m(n + 1)P_n, \end{aligned} \tag{25}$$

where P_n is the probability for the mechanical element to be in the Fock state $|n\rangle$; $\Gamma_{n-1\leftarrow n}$ is the transition rate from $|n\rangle$ to $|n-1\rangle$ induced by the effective magnomechanical coupling. In the weak-coupling regime, the fluctuation spectrum $S_{FF}(\omega) = \int dt e^{i\omega t}\langle F(t)F(0)\rangle$ is determined by the above effective Hamiltonian. According to Fermi's "golden rule," the heating and cooling rate are given by

$$\Gamma_+ = G^2 S_{FF}(-\omega_b), \quad \Gamma_- = G^2 S_{FF}(\omega_b),$$

hence we can obtain the final mean phonon number of the mechanical resonator and the quantum limit of cooling, which read

$$n_f = \frac{\gamma_b n_m + \Gamma_m n_c}{\gamma_b + \Gamma_m}, \quad n_c = \frac{\Gamma_+}{\Gamma_- - \Gamma_+}, \tag{26}$$

where

$$\Gamma_m = G^2[S_{FF}(-\omega_b) - S_{FF}(\omega_b)]$$

is the net cooling rate, and $n_m = (e^{\hbar\omega_b/k_B T} - 1)^{-1}$ is the thermal phonon number with the environmental temperature T.

Figures 5(a) and 5(b) show the fluctuation spectrum $S_{FF}(\omega)$ versus the frequency ω with different magnon-photon coupling strengths g_{ma}. For $\Phi = 0$ (the Hermitian CMM system), increasing the coupling strength leads to the splitting of the single peak into two narrower peaks, with a dip emerging between them [see the dashed and dot-dashed line in Fig. 5(a)], due to the destructive interference between the optical mode and the magnon mode [6]. In particular, for $\Phi = \pi$ (the non-Hermitian CMM system), the fluctuation spectrum $S_{FF}(-\omega_b) \simeq 0$, determining the heating processes, can be achieved near the EP [see the red solid line in Fig. 5(b)]. Accordingly, a factor 2 enhancement of the cooling rate can

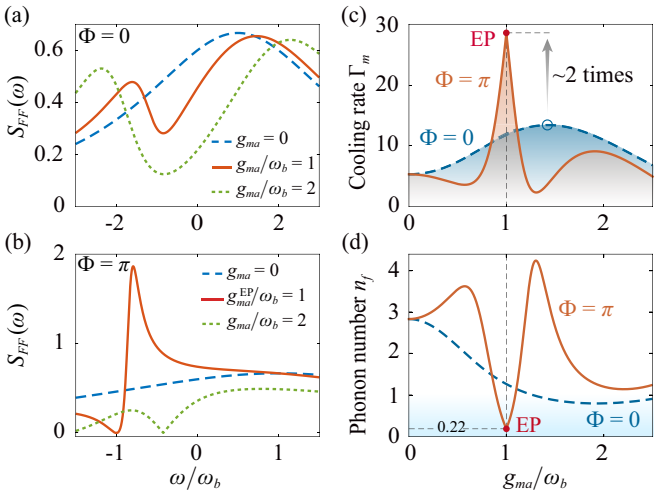

FIG. 5. (a), (b) The fluctuation spectrum $S_{FF}(\omega)$ (in arbitrary units) vs the frequency ω, for different values of the magnon-photon coupling g_{ma}. (c) The net cooling rate $\Gamma_m = \Gamma_- - \Gamma_+$ (in arbitrary units) vs g_{ma}. (d) The mean phonon number n_f vs g_{ma}. Here we have chosen $\kappa_m/\omega_b = 3$ (nonresolved sideband case), and the initial phonon number $n_m = 320$ or $T = 310$ mK. See the text for the other parameter values.

be achievable by approaching the EP [see Fig. 5(c)]. Thus, mechanical cooling deep into the ground state or $n_f \simeq 0.22$ is accessible for such a system precooled down to 310 mK [see Fig. 5(d)]. This opens up the prospect to explore and engineer purely quantum effects of mechanical motion using unconventional CMM devices.

IV. CONCLUSION

In conclusion, we have theoretically studied the role of EPs in a non-Hermitian CMM system, with a tunable dissipative magnon-photon coupling. We find that EPs emerging in such a system can radically change the properties of both photons and phonons. As a result, flexible on-off optical transmission and slow-to-fast light switching are achievable by approaching the EP, which, surprisingly, is also accompanied by enhanced mechanical ground-state cooling, and the main results are summarized in Table I. Also, we note that, in the latest experiment [99], switchable fast-slow light can be realized in a cavity-magnon polariton system by tuning the relative phase of the magnon pumping and cavity probe tones. These results indicate that EP-assisted CMM devices can provide a versatile platform to control coherent interactions of photons, phonons, and magnons, for such a wide range of potential applications as EP-enhanced microwave-to-optical conversion [73], EP-enabled topological energy transfer [64], and improved quantum sensing of weak force or magnetic signal [74–77].

TABLE I. The group delay τ_g under different cases for $\Delta_p = 0$ and $B_0 = 0.07$ mT, and the minimum phonon number n_f under different cases for $T = 310$ mK.

Cases	$\tau_g(\mu s)$	n_f
Hermitian CM	−0.032	
Non-Hermitian CM	0.030	
Hermitian CMM	−93.2	0.78
Non-Hermitian CMM	150	0.22

ACKNOWLEDGMENTS

H.J. is supported by the National Natural Science Foundation of China (Grants No. 11935006 and No. 11774086) and the Science and Technology Innovation Program of Hunan Province (Grant No. 2020RC4047). T.-X.L. is supported in part by Hunan Provincial Innovation Foundation For Postgraduate (Grant No. CX20190339).

[1] Z.-L. Xiang, S. Ashhab, J. Q. You, and F. Nori, Hybrid quantum circuits: Superconducting circuits interacting with other quantum systems, Rev. Mod. Phys. **85**, 623 (2013).
[2] D. Lachance-Quirion, Y. Tabuchi, A. Gloppe, K. Usami, and Y. Nakamura, Hybrid quantum systems based on magnonics, Appl. Phys. Express **12**, 070101 (2019).
[3] C. Kittel, Interaction of spin waves and ultrasonic waves in ferromagnetic crystals, Phys. Rev. **110**, 836 (1958).
[4] H. Huebl, C. W. Zollitsch, J. Lotze, F. Hocke, M. Greifenstein, A. Marx, R. Gross, and S. T. B. Goennenwein, High Cooperativity in Coupled Microwave Resonator Ferrimagnetic Insulator Hybrids, Phys. Rev. Lett. **111**, 127003 (2013).
[5] Y. Tabuchi, S. Ishino, T. Ishikawa, R. Yamazaki, K. Usami, and Y. Nakamura, Hybridizing Ferromagnetic Magnons and Microwave Photons in the Quantum Limit, Phys. Rev. Lett. **113**, 083603 (2014).
[6] X. Zhang, C.-L. Zou, L. Jiang, and H. X. Tang, Strongly Coupled Magnons and Cavity Microwave Photons, Phys. Rev. Lett. **113**, 156401 (2014).
[7] M. Goryachev, W. G. Farr, D. L. Creedon, Y. Fan, M. Kostylev, and M. E. Tobar, High-Cooperativity Cavity QED with Magnons at Microwave Frequencies, Phys. Rev. Applied **2**, 054002 (2014).
[8] L. Bai, M. Harder, Y. P. Chen, X. Fan, J. Q. Xiao, and C.-M. Hu, Spin Pumping in Electrodynamically Coupled Magnon-Photon Systems, Phys. Rev. Lett. **114**, 227201 (2015).
[9] Y. Tabuchi, S. Ishino, A. Noguchi, T. Ishikawa, R. Yamazaki, K. Usami, and Y. Nakamura, Quantum magnonics: The magnon meets the superconducting qubit, C. R. Phys. **17**, 729 (2016).
[10] R. Hisatomi, A. Osada, Y. Tabuchi, T. Ishikawa, A. Noguchi, R. Yamazaki, K. Usami, and Y. Nakamura, Bidirectional conversion between microwave and light via ferromagnetic magnons, Phys. Rev. B **93**, 174427 (2016).
[11] A. Osada, R. Hisatomi, A. Noguchi, Y. Tabuchi, R. Yamazaki, K. Usami, M. Sadgrove, R. Yalla, M. Nomura, and Y. Nakamura, Cavity Optomagnonics with Spin-Orbit Coupled Photons, Phys. Rev. Lett. **116**, 223601 (2016).
[12] X. Zhang, N. Zhu, C.-L. Zou, and H. X. Tang, Optomagnonic Whispering Gallery Microresonators, Phys. Rev. Lett. **117**, 123605 (2016).

[13] J. T. Hou and L. Liu, Strong Coupling between Microwave Photons and Nanomagnet Magnons, Phys. Rev. Lett. **123**, 107702 (2019).

[14] L. Liensberger, A. Kamra, H. Maier-Flaig, S. Geprägs, A. Erb, S. T. B. Goennenwein, R. Gross, W. Belzig, H. Huebl, and M. Weiler, Exchange-Enhanced Ultrastrong Magnon-Magnon Coupling in a Compensated Ferrimagnet, Phys. Rev. Lett. **123**, 117204 (2019).

[15] S. Viola Kusminskiy, H. X. Tang, and F. Marquardt, Coupled spin-light dynamics in cavity optomagnonics, Phys. Rev. A **94**, 033821 (2016).

[16] A. Osada, A. Gloppe, R. Hisatomi, A. Noguchi, R. Yamazaki, M. Nomura, Y. Nakamura, and K. Usami, Brillouin Light Scattering by Magnetic Quasivortices in Cavity Optomagnonics, Phys. Rev. Lett. **120**, 133602 (2018).

[17] J. Xu, C. Zhong, X. Han, D. Jin, L. Jiang, and X. Zhang, Floquet Cavity Electromagnonics, Phys. Rev. Lett. **125**, 237201 (2020).

[18] A. V. Chumak, V. I. Vasyuchka, A. A. Serga, and B. Hillebrands, Magnon spintronics, Nat. Phys. **11**, 453 (2015).

[19] L. Bai, M. Harder, P. Hyde, Z. Zhang, C.-M. Hu, Y. P. Chen, and J. Q. Xiao, Cavity Mediated Manipulation of Distant Spin Currents Using a Cavity-Magnon-Polariton, Phys. Rev. Lett. **118**, 217201 (2017).

[20] Z. Zhang, M. O. Scully, and G. S. Agarwal, Quantum entanglement between two magnon modes via Kerr nonlinearity driven far from equilibrium, Phys. Rev. Research **1**, 023021 (2019).

[21] J. M. P. Nair and G. S. Agarwal, Deterministic quantum entanglement between macroscopic ferrite samples, Appl. Phys. Lett. **117**, 084001 (2020).

[22] M. Harder, L. Bai, P. Hyde, and C.-M. Hu, Topological properties of a coupled spin-photon system induced by damping, Phys. Rev. B **95**, 214411 (2017).

[23] D. Zhang, X.-Q. Luo, Y.-P. Wang, T.-F. Li, and J. Q. You, Observation of the exceptional point in cavity magnon-polaritons, Nat. Commun. **8**, 1368 (2017).

[24] L. V. Abdurakhimov, S. Khan, N. A. Panjwani, J. D. Breeze, M. Mochizuki, S. Seki, Y. Tokura, J. J. L. Morton, and H. Kurebayashi, Magnon-photon coupling in the noncollinear magnetic insulator Cu_2OSeO_3, Phys. Rev. B **99**, 140401(R) (2019).

[25] B. Wang, Z.-X. Liu, C. Kong, H. Xiong, and Y. Wu, Magnon-induced transparency and amplification in $\mathcal{PT}$-symmetric cavity-magnon system, Opt. Express **26**, 20248 (2018).

[26] X. Zhang, C. L. Zou, L. Jiang, and H. X. Tang, Cavity magnomechanics, Sci. Adv. **2**, e1501286 (2016).

[27] J. Gieseler, A. Kabcenell, E. Rosenfeld, J. D. Schaefer, A. Safira, M. J. A. Schuetz, C. Gonzalez-Ballestero, C. C. Rusconi, O. Romero-Isart, and M. D. Lukin, Single-Spin Magnetomechanics with Levitated Micromagnets, Phys. Rev. Lett. **124**, 163604 (2020).

[28] C. Gonzalez-Ballestero, J. Gieseler, and O. Romero-Isart, Quantum Acoustomechanics with a Micromagnet, Phys. Rev. Lett. **124**, 093602 (2020).

[29] J. Li, S.-Y. Zhu, and G. S. Agarwal, Squeezed states of magnons and phonons in cavity magnomechanics, Phys. Rev. A **99**, 021801(R) (2019).

[30] J. Li, S.-Y. Zhu, and G. S. Agarwal, Magnon-Photon-Phonon Entanglement in Cavity Magnomechanics, Phys. Rev. Lett. **121**, 203601 (2018).

[31] J. Li and S.-Y. Zhu, Entangling two magnon modes via magnetostrictive interaction, New J. Phys. **21**, 085001 (2019).

[32] M. Yu, H. Shen, and J. Li, Magnetostrictively Induced Stationary Entanglement between Two Microwave Fields, Phys. Rev. Lett. **124**, 213604 (2020).

[33] S.-N. Huai, Y.-L. Liu, J. Zhang, L. Yang, and Y.-X. Liu, Enhanced sideband responses in a $\mathcal{PT}$-symmetric-like cavity magnomechanical system, Phys. Rev. A **99**, 043803 (2019).

[34] C. Kong, B. Wang, Z.-X. Liu, H. Xiong, and Y. Wu, Magnetically controllable slow light based on magnetostrictive forces, Opt. Express **27**, 5544 (2019).

[35] M. F. Colombano, G. Arregui, F. Bonell, N. E. Capuj, E. Chavez-Angel, A. Pitanti, S. O. Valenzuela, C. M. Sotomayor-Torres, D. Navarro-Urrios, and M. V. Costache, Ferromagnetic Resonance Assisted Optomechanical Magnetometer, Phys. Rev. Lett. **125**, 147201 (2020).

[36] P. Peng, W. Cao, C. Shen, W. Qu, J. Wen, L. Jiang, and Y. Xiao, Anti-parity-time symmetry with flying atoms, Nat. Phys. **12**, 1139 (2016).

[37] Y. Jiang, Y. Mei, Y. Zuo, Y. Zhai, J. Li, J. Wen, and S. Du, Anti-Parity-Time Symmetric Optical Four-Wave Mixing in Cold Atoms, Phys. Rev. Lett. **123**, 193604 (2019).

[38] Y. Choi, C. Hahn, J. W. Yoon, and S. H. Song, Observation of an anti-PT-symmetric exceptional point and energy-difference conserving dynamics in electrical circuit resonators, Nat. Commun. **9**, 2182 (2018).

[39] Y. Li, Y.-G. Peng, L. Han, M.-A. Miri, W. Li, M. Xiao, X.-F. Zhu, J. Zhao, A. Alú, S. Fan, and C.-W. Qiu, Anti-parity-time symmetry in diffusive systems, Science **364**, 170 (2019).

[40] X.-L. Zhang, T. Jiang, and C. T. Chan, Dynamically encircling an exceptional point in anti-parity-time symmetric systems: Asymmetric mode switching for symmetry-broken modes, Light Sci. Appl. **8**, 88 (2019).

[41] Q. Li, C.-J. Zhang, Z.-D. Cheng, W.-Z. Liu, J.-F. Wang, F.-F. Yan, Z.-H. Lin, Y. Xiao, K. Sun, Y.-T. Wang, J.-S. Tang, J.-S. Xu, C.-F. Li, and G.-C. Guo, Experimental simulation of anti-parity-time symmetric lorentz dynamics, Optica **6**, 67 (2019).

[42] H. Fan, J. Chen, Z. Zhao, J. Wen, and Y.-P. Huang, Antiparity-time symmetry in passive nanophotonics, ACS Photon. **7**, 3035 (2020).

[43] H. Zhang, R. Huang, S.-D. Zhang, Y. Li, C.-W. Qiu, F. Nori, and H. Jing, Breaking Anti-PT symmetry by spinning a resonator, Nano Lett. **20**, 7594 (2020).

[44] Y.-P. Wang and C.-M. Hu, Dissipative couplings in cavity magnonics, J. Appl. Phys. **127**, 130901 (2020).

[45] M. Harder, Y. Yang, B. M. Yao, C. H. Yu, J. W. Rao, Y. S. Gui, R. L. Stamps, and C.-M. Hu, Level Attraction Due to Dissipative Magnon-Photon Coupling, Phys. Rev. Lett. **121**, 137203 (2018).

[46] P.-C. Xu, J. W. Rao, Y. S. Gui, X. Jin, and C.-M. Hu, Cavity-mediated dissipative coupling of distant magnetic moments: Theory and experiment, Phys. Rev. B **100**, 094415 (2019).

[47] C. H. Yu, Y. Yang, J. W. Rao, P. Hyde, Y.-P. Wang, B. Zhang, Y. S. Gui, and C.-M. Hu, Spin number dependent dissipative coupling strength, AIP Adv. **9**, 115012 (2019).

[48] B. Bhoi, B. Kim, S.-H. Jang, J. Kim, J. Yang, Y.-J. Cho, and S.-K. Kim, Abnormal anticrossing effect in photon-magnon coupling, Phys. Rev. B **99**, 134426 (2019).

[49] Y. Yang, J. W. Rao, Y. S. Gui, B. M. Yao, W. Lu, and C.-M. Hu, Control of the Magnon-Photon Level Attraction in a Planar Cavity, Phys. Rev. Applied **11**, 054023 (2019).

[50] J. W. Rao, C. H. Yu, Y. T. Zhao, Y. S. Gui, X. L. Fan, D. S. Xue, and C.-M. Hu, Level attraction and level repulsion of magnon coupled with a cavity anti-resonance, New J. Phys. **21**, 065001 (2019).

[51] J. W. Rao, Y. P. Wang, Y. Yang, T. Yu, Y. S. Gui, X. L. Fan, D. S. Xue, and C.-M. Hu, Interactions between a magnon mode and a cavity photon mode mediated by traveling photons, Phys. Rev. B **101**, 064404 (2020).

[52] B. Yao, T. Yu, X. Zhang, W. Lu, Y. Gui, C.-M. Hu, and Y. M. Blanter, The microscopic origin of magnon-photon level attraction by traveling waves: Theory and experiment, Phys. Rev. B **100**, 214426 (2019).

[53] B. Yao, T. Yu, Y. S. Gui, J. W. Rao, Y. T. Zhao, W. Lu, and C. M. Hu, Coherent control of magnon radiative damping with local photon states, Commun. Phys. **2**, 161 (2019).

[54] Y.-P. Wang, J. W. Rao, Y. Yang, P.-C. Xu, Y. S. Gui, B. M. Yao, J. Q. You, and C.-M. Hu, Nonreciprocity and Unidirectional Invisibility in Cavity Magnonics, Phys. Rev. Lett. **123**, 127202 (2019).

[55] Y. T. Zhao, J. W. Rao, Y. S. Gui, Y. P. Wang, and C.-M. Hu, Broadband Nonreciprocity Realized by Locally Controlling the Magnon's Radiation, Phys. Rev. Applied **14**, 014035 (2020).

[56] H. Y. Yuan, P. Yan, S. Zheng, Q. Y. He, K. Xia, and M.-H. Yung, Steady Bell State Generation via Magnon-Photon Coupling, Phys. Rev. Lett. **124**, 053602 (2020).

[57] J. Zhao, Y. Liu, L. Wu, C.-K. Duan, Y.-x. Liu, and J. Du, Observation of Anti-$\mathcal{PT}$-Symmetry Phase Transition in the Magnon-Cavity-Magnon Coupled System, Phys. Rev. Applied **13**, 014053 (2020).

[58] Y. Yang, Y.-P. Wang, J. W. Rao, Y. S. Gui, B. M. Yao, W. Lu, and C.-M. Hu, Unconventional Singularity in Anti-Parity-Time Symmetric Cavity Magnonics, Phys. Rev. Lett. **125**, 147202 (2020).

[59] M.-A. Miri and A. Alù, Exceptional points in optics and photonics, Science **363**, eaar7709 (2019).

[60] Ş. K. Özdemir, S. Rotter, F. Nori, and L. Yang, Parity-time symmetry and exceptional points in photonics, Nat. Mater. **18**, 783 (2019).

[61] J. Wen, X. Jiang, L. Jiang, and M. Xiao, Parity-time symmetry in optical microcavity systems, J. Phys. B **51**, 222001 (2018).

[62] H. Hodaei, M.-A. Miri, M. Heinrich, D. N. Christodoulides, and M. Khajavikhan, Parity-time-symmetric microring lasers, Science **346**, 975 (2014).

[63] L. Feng, Z. J. Wong, R.-M. Ma, Y. Wang, and X. Zhang, Single-mode laser by parity-time symmetry breaking, Science **346**, 972 (2014).

[64] H. Xu, D. Mason, L. Jiang, and J. G. E. Harris, Topological energy transfer in an optomechanical system with exceptional points, Nature (London) **537**, 80 (2016).

[65] S. Assawaworrarit, X. Yu, and S. Fan, Robust wireless power transfer using a nonlinear parity-time-symmetric circuit, Nature (London) **546**, 387 (2017).

[66] L. Feng, M. Ayache, J. Huang, Y. L. Xu, M. H. Lu, Y. F. Chen, Y. Fainman, and A. Scherer, Nonreciprocal light propagation in a silicon photonic circuit, Science **333**, 729 (2011).

[67] B. Peng, Ş. K. Özdemir, F. Lei, F. Monifi, M. Gianfreda, G. Long, S. Fan, F. Nori, C. Bender, and L. Yang, Parity-time-symmetric whispering-gallery microcavities, Nat. Phys. **10**, 394 (2014).

[68] Q. Zhong, S. Nelson, Ş. K. Özdemir, and R. El-Ganainy, Controlling directional absorption with chiral exceptional surfaces, Opt. Lett. **44**, 5242 (2019).

[69] H. Hodaei, A. U. Hassan, S. Wittek, H. Garcia-Gracia, R. El-Ganainy, D. N. Christodoulides, and M. Khajavikhan, Enhanced sensitivity at higher-order exceptional points, Nature (London) **548**, 187 (2017).

[70] P.-Y. Chen, M. Sakhdari, M. Hajizadegan, Q. Cui, M. M.-C. Cheng, R. El-Ganainy, and A. Alù, Generalized parity-time symmetry condition for enhanced sensor telemetry, Nat. Electron. **1**, 297 (2018).

[71] Z. Dong, Z. Li, F. Yang, C.-W. Qiu, and J. S. Ho, Sensitive readout of implantable microsensors using a wireless system locked to an exceptional point, Nat. Electron. **2**, 335 (2019).

[72] Z. Xiao, H. Li, T. Kottos, and A. Alù, Enhanced Sensing and Nondegraded Thermal Noise Performance Based on $\mathcal{PT}$-Symmetric Electronic Circuits with a Sixth-Order Exceptional Point, Phys. Rev. Lett. **123**, 213901 (2019).

[73] Y. S. Ihn, S.-Y. Lee, D. Kim, S. H. Yim, and Z. Kim, Coherent multimode conversion from microwave to optical wave via a magnon-cavity hybrid system, Phys. Rev. B **102**, 064418 (2020).

[74] T. Trickle, Z. Zhang, and K. M. Zurek, Detecting Light Dark Matter with Magnons, Phys. Rev. Lett. **124**, 201801 (2020).

[75] S. P. Wolski, D. Lachance-Quirion, Y. Tabuchi, S. Kono, A. Noguchi, K. Usami, and Y. Nakamura, Dissipation-Based Quantum Sensing of Magnons with a Superconducting Qubit, Phys. Rev. Lett. **125**, 117701 (2020).

[76] C. A. Potts, V. A. S. V. Bittencourt, S. V. Kusminskiy, and J. P. Davis, Magnon-Phonon Quantum Correlation Thermometry, Phys. Rev. Applied **13**, 064001 (2020).

[77] M. S. Ebrahimi, A. Motazedifard, and M. B. Harouni, Ultra-precision single-quadrature quantum magnetometry in cavity electromagnonics, arXiv:2011.06081.

[78] T. Gilbert, A phenomenological theory of damping in ferromagnetic materials, IEEE Trans. Magn. **40**, 3443 (2004).

[79] V. N. Krivoruchko, Spin waves damping in nanometre-scale magnetic materials (review article), Low Temp. Phys. **41**, 670 (2015).

[80] M. A. W. Schoen, D. Thonig, M. L. Schneider, T. J. Silva, H. T. Nembach, O. Eriksson, O. Karis, and J. M. Shaw, Ultra-low magnetic damping of a metallic ferromagnet, Nat. Phys. **12**, 839 (2016).

[81] V. L. Safonov, Tensor form of magnetization damping, J. Appl. Phys. **91**, 8653 (2002).

[82] H. Bertram, Z. Jin, and V. Safonov, Experimental and theoretical studies of thermal magnetization noise in GMR heads, IEEE Trans. Magn. **38**, 38 (2002).

[83] H. Bertram, V. Safonov, and Z. Jin, Thermal magnetization noise, damping fundamentals, and mode analysis: Application to a thin film GMR sensor, IEEE Trans. Magn. **38**, 2514 (2002).

[84] L. Chen, S. Mankovsky, S. Wimmer, M. A. W. Schoen, H. S. Körner, M. Kronseder, D. Schuh, D. Bougeard, H. Ebert, D. Weiss, and C. H. Back, Emergence of anisotropic Gilbert damping in ultrathin Fe layers on GaAs(001), Nat. Phys. **14**, 490 (2018).

[85] M. Harder, L. Bai, C. Match, J. Sirker, and C.-M. Hu, Study of the cavity-magnon-polariton transmission line shape, Sci. China Phys., Mech. Astron. **59**, 117511 (2016).

[86] K.-J. Boller, A. Imamoglu, and S. E. Harris, Observation of Electromagnetically Induced Transparency, Phys. Rev. Lett. **66**, 2593 (1991).

[87] G. S. Agarwal and S. Huang, Electromagnetically induced transparency in mechanical effects of light, Phys. Rev. A **81**, 041803(R) (2010).

[88] S. Weis, R. Rivière, S. Deléglise, E. Gavartin, O. Arcizet, A. Schliesser, and T. J. Kippenberg, Optomechanically induced transparency, Science **330**, 1520 (2010).

[89] H. Jing, Ş. K. Özdemir, H. Lü, and F. Nori, High-order exceptional points in optomechanics, Sci. Rep. **7**, 3386 (2017).

[90] C. Fabre, M. Pinard, S. Bourzeix, A. Heidmann, E. Giacobino, and S. Reynaud, Quantum-noise reduction using a cavity with a movable mirror, Phys. Rev. A **49**, 1337 (1994).

[91] C. W. Gardiner and M. J. Collett, Input and output in damped quantum systems: Quantum stochastic differential equations and the master equation, Phys. Rev. A **31**, 3761 (1985).

[92] H. Jing, Ş. K. Özdemir, Z. Geng, J. Zhang, X.-Y. Lü, B. Peng, L. Yang, and F. Nori, Optomechanically-induced transparency in parity-time-symmetric microresonators, Sci. Rep. **5**, 9663 (2015).

[93] H. Lü, C. Wang, L. Yang, and H. Jing, Optomechanically Induced Transparency at Exceptional Points, Phys. Rev. Applied **10**, 014006 (2018).

[94] H. Zhang, F. Saif, Y. Jiao, and H. Jing, Loss-induced transparency in optomechanics, Opt. Express **26**, 25199 (2018).

[95] A. H. Safavi-Naeini, T. P. M. Alegre, J. Chan, M. Eichenfield, M. Winger, Q. Lin, J. T. Hill, D. E. Chang, and O. Painter, Electromagnetically induced transparency and slow light with optomechanics, Nature (London) **472**, 69 (2011).

[96] X. Zhou, F. Hocke, A. Schliesser, A. Marx, H. Huebl, R. Gross, and T. J. Kippenberg, Slowing, advancing and switching of microwave signals using circuit nanoelectromechanics, Nat. Phys. **9**, 179 (2013).

[97] I. Wilson-Rae, N. Nooshi, W. Zwerger, and T. J. Kippenberg, Theory of Ground State Cooling of a Mechanical Oscillator Using Dynamical Backaction, Phys. Rev. Lett. **99**, 093901 (2007).

[98] A. A. Clerk, M. H. Devoret, S. M. Girvin, F. Marquardt, and R. J. Schoelkopf, Introduction to quantum noise, measurement, and amplification, Rev. Mod. Phys. **82**, 1155 (2010).

[99] J. Zhao, L. Wu, T. Li, Y.-X. Liu, F. Nori, Y. Liu, and J. Du, Phase-Controlled Pathway Interferences and Switchable Fast-Slow Light in a Cavity-Magnon Polariton System, Phys. Rev. Applied **15**, 024056 (2021).